Materials and Design 186 (2020) 108315

Contents lists available at ScienceDirect

Materials and Design

journal homepage: www.elsevier.com/locate/matdes

Fiber reinforced alkali-activated stone wool composites fabricated by hot-pressing technique

Hoang Nguyen [a,*], Alexandra Kaas [b], Paivo Kinnunen [a], Valter Carvelli [c], Carol Monticelli [c], Juho Yliniemi [a], Mirja Illikainen [a]

[a] Fibre and Particle Engineering Research Unit, University of Oulu, Pentti Kaiteran Katu 1, 90014, Oulu, Finland
[b] Institute of Mechanical Process Engineering and Mineral Processing, Technical University Bergakademie Freiberg, Agricolastraße 1, 09599, Freiberg, Germany
[c] Department A.B.C., Politecnico di Milano, Piazza Leonardo Da Vinci 32, 20133, Milan, Italy

HIGHLIGHTS

- High performance cementitious composites were fabricated by hot-pressing technique with rapid strength development.
- Hot-pressed composites released less CO_2 (by 18–20 %) than the conventional oven-cured material.
- Hot-pressed mixtures obtained top 3 best balanced compositions among mechanical properties, cost, and environmental impact.
- Some damages on fibers were observed when pressing at 120 °C due to a synergistic effect of high pressure and temperature.

GRAPHICAL ABSTRACT

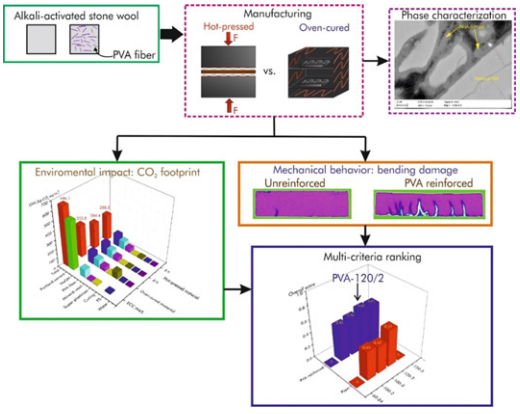

ARTICLE INFO

Article history:
Received 18 July 2019
Received in revised form 23 September 2019
Accepted 27 October 2019
Available online 9 November 2019

Keywords:
Hot-pressing
Alkali-activated material
High performance cementitious composite
Mineral wool
Recycling

ABSTRACT

Cementitious composite that has short molding time and high mechanical performance is favorable in pre-cast concrete industry. In this context, this study reports the use of hot-pressing technique to fabricate PVA fiber reinforced composites using alkali-activated stone wool (a waste from building insulation). Eight different mixtures were developed by varying the pressing time and temperature in comparison to the conventional oven-cured alkali-activated material. The mechanical performance of all compositions was evaluated under bending and compressive loadings. Life cycle assessment was used to investigate the greenhouse gas emission and embodied energy of the developed composites. The results reveal that PVA fibers greatly enhanced the mechanical performance of all reinforced mixtures with deflection hardening behavior and improvement in compressive strength. The hot-pressing technique lowered CO_2 emission and saved energy. Finally, a multi-criteria ranking method suggests hot-pressed PVA fiber reinforced cementitious composite, manufactured at 120 °C for 2 h, is the best composition attaining balance among energy spent, mechanical properties, and CO_2 footprint.

1. Introduction

Alkali-activated material (AAM) has been highlighted as an alternative to partially replace ordinary and blended Portland cement (PC). AAM was reported to have comparable mechanical properties with

* Corresponding author.
E-mail address: hoang.nguyen@oulu.fi (H. Nguyen).

https://doi.org/10.1016/j.matdes.2019.108315

Table 1
Chemical composition (wt%) of SW measured by XRF.

Na_2O	MgO	Al_2O_3	SiO_2	CaO	Fe_2O_3	K_2O	MnO	Others	LOI
1.3	11.6	15.4	38.9	18.3	11.1	0.4	0.2	2.8	1.7

lower CO_2 emissions compared to OPC [1,2]. In addition, the development of AAM from industrial by-products is highly encouraged due to both economic and environmental benefits. While fly ashes and slags seems to be commonly-used precursors for AAM manufacturing [3,4], stone wool (SW—a waste from building insulation materials) is a largely under-utilized material. Over 2 million tons of this by-product is generated each year in Europe alone and the amount is expected to increase [5]. Moreover, as SW is made at high temperatures by melting quartz sand, basalt, dolomite [6], its composition contains oxides of Si, Ca, Mg and Al. Therefore, using SW as a precursor to produce AAM is of immediate interest.

Polymeric fibers (e.g., PVA, PP, and PE) are usually employed to reinforce AAM for better mechanical performance. The fibers are able to improve the mechanical properties of reinforced AAM with pseudo strain hardening (PSH) behavior and reduce the brittleness of the material [7–11]. The development of strain hardening fiber reinforced AAM composite is well reported in the literature [12,13]. With the presence of fibers, crack propagation is delayed via fiber bridging action. As a result, the loading of fiber reinforced composite generates multiple cracks with changes in post-peak behavior. Moreover, the current development of cementitious composites has been enabling multiple applications such as piezoresistive composite using carbon black and rubber fibers [14], 3D-printed strain hardening cementitious composites [15].

As for manufacturing of pre-cast AAM in construction, conventional low-calcium AAM is commonly cured at elevated temperature (around 60–80 °C) for 24 h before demolding. To shorten the molding time while still attaining high mechanical properties, Ranjbar et al. [16,17] proposed a combination of high temperature and pressure to fabricate fly ash based AAM. The hot-pressing technique is favorable to produce a dense structure and eventually high compressive strength in a very short time (approximately 20 min) [16,18]. However, with such high manufacturing temperature (i.e., 350 °C [16]), most polymeric fibers will be completely decomposed or damaged; hence, the effects of fibrous reinforcement are not achieved in reinforced AAM. In addition, the high temperature is more challenging to handle at large scale (e.g., mass production), and the energy consumption to operate at that temperature can be prohibitive. Consequently, using hot-pressing technique to produce high performance fiber reinforced AAM at relatively low temperature is beneficial and interesting in terms of manufacturing process and quick strength development.

The reaction of AAM at high temperature and pressure are of interest and not yet well established. It is well-known that AAMs are formed through the reaction of alkali activator, water, and aluminosilicate precursors [19]. The main reaction product is mainly a calcium (alkali) aluminosilicate hydrate (C–(N–)A–S–H) gel [20], which is distinguishable with calcium (alumino)silicate hydrate (C–(A–)S–H) gel in hydrated PC [21]. Along with this reaction gel, AAM contains also other products (e.g., Mg–Al layered double hydroxide and AFm phases), which have different thermodynamic properties and eventually can play important role in hardened AAMs [22]. In addition, as reported recently by Kuenzel and Ranjbar [23], temperature (25–145 °C) and exposing time (2–24 h) dominated the dissolution rates of fly ash in NaOH-based AAM rather than NaOH molarity. Therefore, the effects of fabricating technique (i.e., hot-pressing vs. oven-cured procedure) on the phase assemblage of AAMs need more understanding, especially in the case of the underutilized SW.

In this context, the present study focuses on the development of a high-performance fiber reinforced AAM from SW composite manufactured by hot-pressing technique. It intends to provide detailed understandings of:

- the effects of pressing time and temperature on the strength development, mechanical properties, phase assemblage, and microstructure at early and final stage of hot-press process, via mechanical testing under bending and compressive loadings and phase characterization including X-ray diffraction (XRD), scanning electron microscope (SEM), and differential thermogravimetry (DTG);
- whether the hot-pressing can reduce CO_2 footprint and lower the embodied energy in comparison to oven-cured AAM via life cycle assessment (LCA);
- the most balanced curing procedure in terms of mechanical properties, economic and environmental benefits, employing a multi-criteria ranking method.

In comparison to Refs. [16,17], in which fibers were not considered, a lower pressing temperature was used in this study to enable the use of PVA fibers as reinforcement and to produce high performance fiber reinforced cementitious composites. To the authors' knowledge, this is the first attempt to manufacture a fiber reinforced alkali-activated SW composite with hot-pressing technique. By shortening the mold cycle, production capacity can be increased compared to the conventional

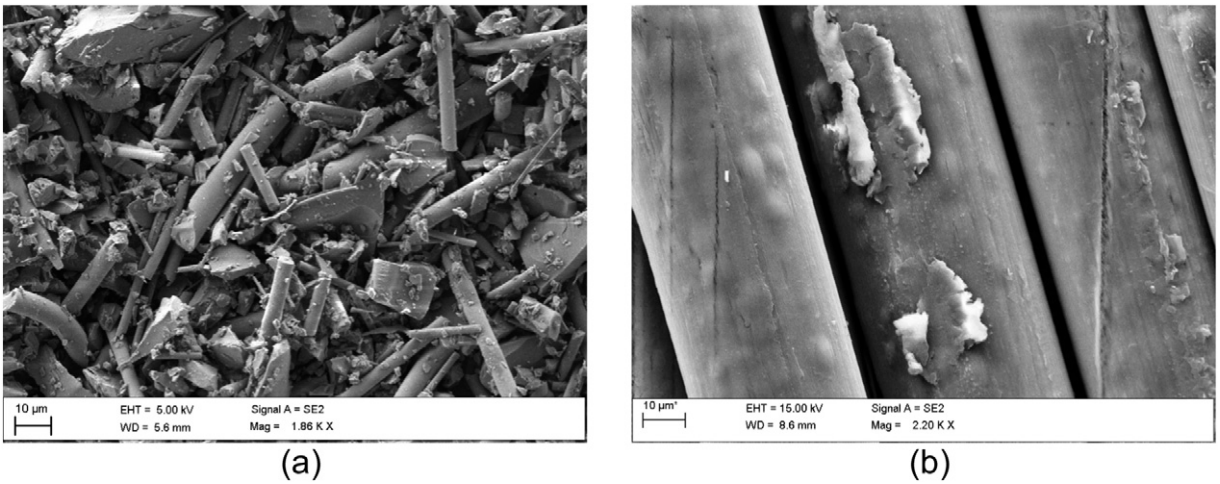

Fig. 1. SEM images of (a) ground SW and (b) PVA fiber.

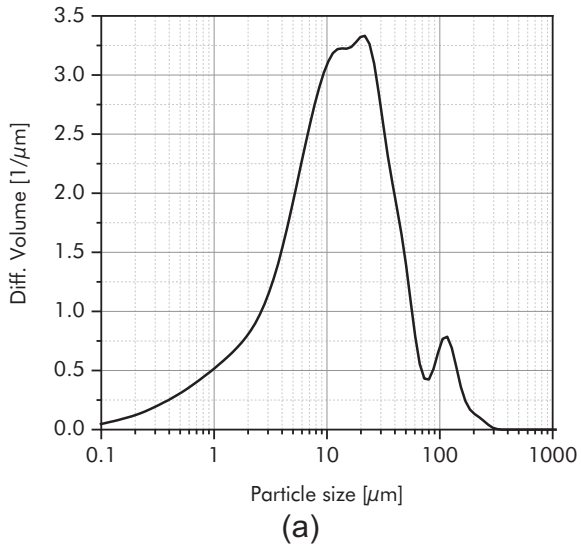

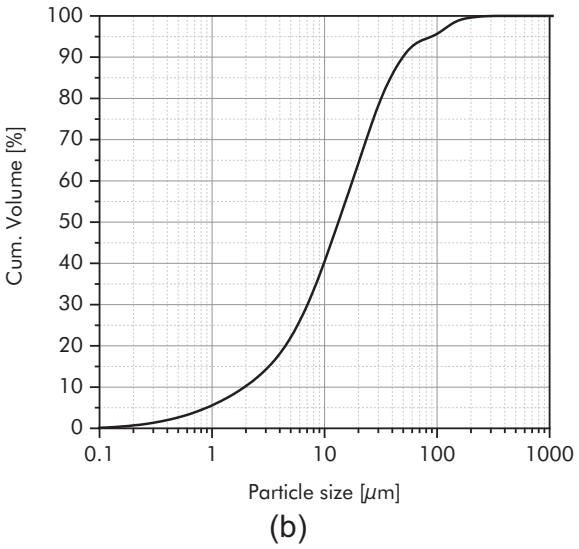

technique. Consequently, it is possible to save energy per manufactured product.

2. Materials and manufacturing

2.1. Materials

In this study SW from Paroc Group Oy, Finland was used. The chemical composition of SW was analyzed by X-ray fluorescence spectroscopy (XRF) (PANalytical Omnian Axiosmax) shown in Table 1. Due to fibrous nature of SW, the raw material was milled according to the following steps. First, a portion of 200 g of SW was milled for 15 min at a speed of 6000 rpm in a 10 L chamber with a ball filling ratio of 11%. Afterwards, the same portion of SW was added into the chamber repeating 5 times and milled in the same conditions with the previous step. The SEM image of milled SW (Fig. 1a) shows the needle-like shape of particle, caused by the fibrous nature of the raw material. The particle size distribution of milled SW was checked periodically by laser diffraction method with Fraunhofer model [24] to obtain a median particle size d_{50} of about 10 μm, which is similar to OPC (Fig. 2). In addition, it is worth noting that the diffractive distribution (Fig. 2a) of SW shows a bimodal distribution, in which there are 2 peaks at 22 and 116 μm showing two means of the distribution. Possibilities can be due to the needle shape of the particles and agglomeration of the fibers during measurement. Moreover, it is challenging to measure precisely the d_{50} of milled SW due to the fibrous shape of the material.

PVA fibers were used as reinforcement (Fig. 1b) being a good compromise in mechanical properties. Physical and mechanical properties are detailed in Table 2. According to Ref. [12], the minimum fiber volume fraction was 2%, as adopted in the present study, to yield PSH behavior in reinforced geopolymer. As for aggregate, fine sand (FS) was used to obtain good fiber dispersant as discussed in Ref. [25]. Standard sand (DIN EN 196-1) was milled for 1 h at 6000 rpm with filling ratio of 60% to achieve fine sand (FS) (d_{50} around 100 μm). Naphthalene sulfonate-based superplasticizer (Mighty 100, provided by KAO, Japan; and here named M100) was used as a powdered chemical. It is appropriate for alkali-activated system according to preliminary experiments.

2.2. Manufacturing of fiber reinforced cementitious composite

The mortar for the specimens was prepared according to the following steps. Alkaline solution NaOH was produced by weighting NaOH pellets (product code: 28245.460, supplied by VWR Finland) and dissolving in deionized water using magnetic stirring speed 7000 rpm for 10 min. A 5 M solution was prepared based on preliminary experiment in which the activator was designed to obtain compressive strength of 35–40 MPa after 28 days. The solution was cooled down to room temperature in a sealed plastic bottle for at least 24 h prior to the use. The mix recipes of plain and reinforced compositions are shown in Table 3. SW, superplasticizer M100 and FS were weighted and mixed together in a Kenwood 5 L mixer at low (100 rpm) and high (200 rpm) speed for 1 min each level. Alkaline solution is weighted and gradually added to the mix dry powder and mixed for 1 min at low and for 2 min at high speed. For the mortar with reinforcement, PVA fibers were added gradually during 15 min mixing period at high speed to prevent fiber clutching and balling in mortars. The finished mortar was casted in an oiled mold.

As for hot-pressed mixtures, after casting into a mold, mortars were hot pressed with a Fontijne Presses (LABECON 300, the Netherlands). A mold was made of stainless steel and assembled to have expected shape as shown in Fig. 3. The mold was cured between two plates in the machine for 2 or 3 h at 100 or 120 °C by a fixed pressing force of 60 kN (roughly a pressure of 25 MPa), which was controlled automatically. It is worth noting that the pressing temperatures were chosen to be quite lower than the onset of PVA degradation (i.e., roughly 180 °C [26]), while the pressing times were adopted after preliminary measurements to get a good compromise of mechanical properties and short molding time. In addition, samples cured in oven were considered for comparison with the hot-pressed compositions. Oven-cured mixtures were vibrated for 3 min at 1 Hz and cured in an oven at 60 °C for 24 h. After demolding (i.e., 2 and 3 h for hot-pressed samples and 24 h for oven-cured samples), both hot-pressed and oven-cured samples were stored in plastic bags. The materials' ID are shown in Table 4 to distinguish different curing conditions and compositions. Phase characterization and mechanical tests of all mixtures were conducted 1 h after demolding, and after 40 and 60 days of hydration at room temperature.

3. Features of material characterization and mechanical tests

XRD analysis was performed on a Rigaku SmartLab 9 kW (Japan) at 40 kV. The analysis used Co Kα radiation ($K\alpha1 = 1.78892$ Å; $K\alpha2 = 1.79278$ Å; $K\alpha1/K\alpha2 = 0.5$), at a scan rate of 4°/min in the range 5°–90° (2θ), and 0.02°/step. Phase identification was done using "X'pert HighScore Plus" (PANalytical software).

DTG was used to obtain some understanding of the phase composition and reaction product of the developed materials. Prior to the

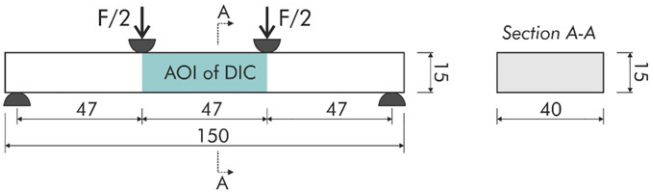

Fig. 3. Scheme of the 4-point bending test with the area of interest (AOI) for the digital image correlation (DIC) marked in light blue; dimensions are in mm.

measurement, samples after 60 days of reaction were dried in oven at 60 °C for 24 h. Approximately 50 mg of dried samples were crushed into powder, transferred to corundum crucibles and heated from room temperature (23–24 °C) up to 1000 °C at the rate of 5 °C/min in nitrogen environment with a flow rate of 20 ml/min.

The microstructure of materials was observed and analyzed by SEM using backscattered electrons (BSE) and energy dispersive X-ray (EDS) in a Zeiss Ultra Plus (Germany). The accelerating voltage and working distance were set to 15 kV and 7–8.5 mm, respectively. Hydration stoppage was done on mortar samples by solvent exchange with isopropanol. Samples were impregnated to epoxy resin under vacuum, and then polished with diamond polishing papers ranging from 220 to 1 μm with a speed of 150 rpm. Ethanol was used during polishing process to prevent further hydration.

Regarding mechanical testing for the developed mixtures, quasi-static 4-point flexural and uniaxial compressive tests were employed. The bending and compressive tests were conducted by Zwick devices (load cell from 10 to 100 kN). Fig. 3 shows the scheme of the flexural test and the geometry of specimen. Four specimens for each combination were tested to determine the flexural property and performance of the mixtures. The 4-point bending test was controlled by displacement at a rate of 0.4 mm/min. The flexural strength and modulus of elasticity were calculated according to ASTM and ISO standards [27,28]:

$$\sigma_f = \frac{FL^2}{bh} \quad (1)$$

$$E_f = \frac{0.21L^3}{bh}\left(\frac{\Delta F}{\Delta s}\right) \quad (2)$$

where: σ_f and E_f is flexural strength and flexural modulus of elasticity, respectively; F is maximum load; L is span; b and h are width and high of the specimen, respectively; ΔF and Δs are the difference in load and the corresponding deflection at the two levels of flexural strain as suggested in the adopted standards. The compressive strength was measured, after bending failure, by loading halves of the prismatic bending specimens with an area of 20 × 20 mm^2. Four compression tests were done for each material with a displacement rate of 1 mm/min.

Digital image correlation (DIC) technique was used along with flexural tests to monitor the cracks pattern evolution on one longitudinal lateral surface. Images (with acquisition frequency of 1 Hz) were captured and analyzed by LaVision StrainMaster [29] on the area of interest (AOI) of samples indicated in Fig. 3. The sample's surface was white-painted with randomly-distributed black acrylic paint dots. The aperture and the shutter speed of camera were set to f/4.0 and 2000 μs, respectively. DIC processing provides full-field displacement measurement, as well as the cracks opening displacement (COD) adopted in the following for comparison. The subset and step size of image processing was 31 and 5, respectively.

After the mechanical testing, the morphology of fibers and matrices was observed on the fracture surface of specimens by secondary electron SEM on a Zeiss Sigma (Germany). The voltage was set to 5 kV, and samples were bagged cured and coated with a 70 nm Pt layer prior to the observation.

Table 4
ID of different alkali-activated SW mixtures.

Time [h]	Temperature [°C]		
	60	100	120
2		100/2 PVA-100/2	120/2 PVA-120/2
3	–	100/3 PVA-100/3	120/3 PVA-120/3
24	60/24 PVA-60/24	–	–

4. Results and discussion

The mechanical properties of the developed cementitious composites via hot-pressing technique are detailed in comparison to the conventional oven-cured one. The comparisons are based on three main aspects: the eft of hot-press and oven curing on the hydration and mechanical properties, the effect of hot-press timing and temperature on the mechanical behavior, and the effect of PVA fiber reinforcement on the composites.

4.1. Phase characterization

The main reaction product of all prepared samples is likely amorphous calcium (sodium) aluminate silicate hydrate (C–(N–)A–S–H) gel (Fig. 4). A broad reflection near 34° 2θ is visible in the X-ray diffractograms which most likely indicates the presence of C–(N–)A–S–H gel. The only crystalline phase identified was quartz (PDF: 04-014-7568) originating from the sand used as aggregate. The SEM-BSE image of the developed materials (Fig. 5a) clearly indicates the outer and inner reaction gel surrounding the residual SW particles. The rim was also reported in NaOH activated slag-based binder, which had a denser hydration gel, and more pores were visible in the matrix at later ages [30]. In addition, the ternary Na-Si-Al atomic plots based on SEM with EDS point analyses confirm the presence of an intermixed C–(N–)A–S–H gels in both oven-cured and hot-pressed mixtures (Fig. 5b –c). It is worth mentioning that the atomic percentage of Ca ranged from 20 to 80% of the intermixed composition, while there was negligible difference in the cloud data of the ternary Na-Si-Al atomic among mixtures. However, the intermixed of gel in hot-pressed composition at 100 °C leaned toward higher atomic percentage of Na (Fig. 5c). This suggests having further investigations on the effects of temperature and pressing time on the phase assemblage of hot-pressed mixtures via thermodynamic perspective.

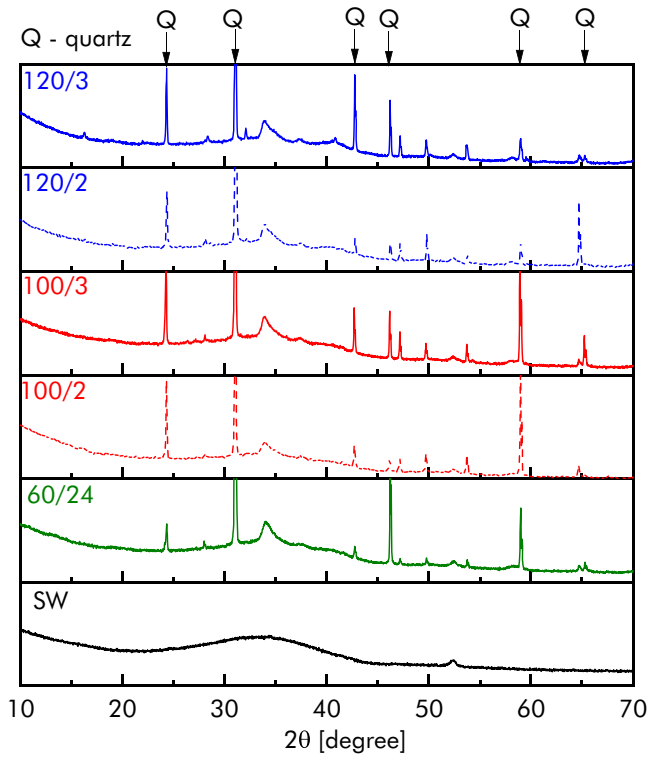

Fig. 4. XRD characterization of all mixtures compared to the raw SW material after 60 days of hydration.

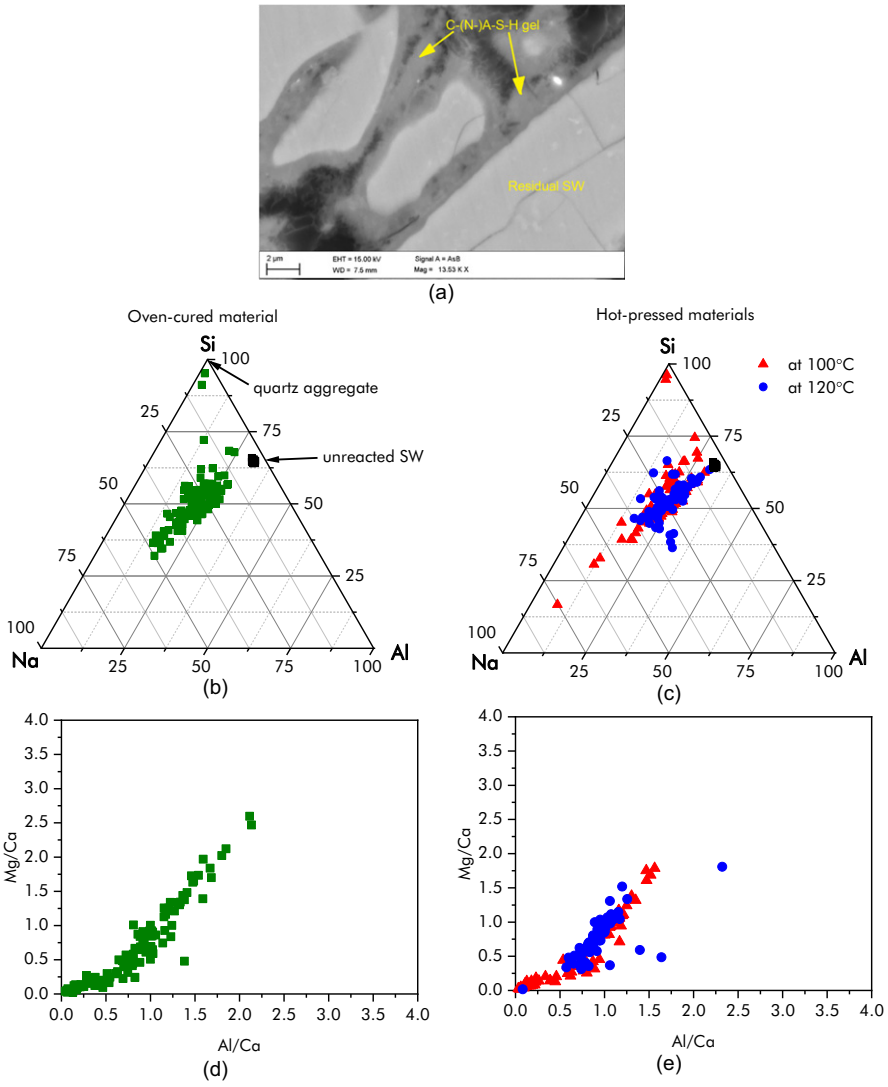

Fig. 5. (a) Representative SEM-BSE image of the alkali-activated SW, (b–c) ternary plot of Na-Si-Al atomic percentage, and (d–e) Mg/Ca vs. Al/Ca atomic ratio of mortar samples from SEM-EDS analyses.

Fig. 6 shows the DTG and TG results for the prepared materials (see Table 4) and original SW. The slight mass loss up to 110 °C indicates evaporation of loosely bound water and remaining free water present in the pores of the hardened gel. The mass loss between 150 and 300 °C is associated with the evaporation of the physically absorbed water from the reaction products (i.e. C–(N–)A–S–H and/or C–S–H-type gels) [31]. The samples prepared at 120 °C show much lower weight loss up to 150 °C than other samples, which is likely due loosely bound water and pore water evaporation during sample preparation. On the other hand, the mass loss between 300° and 700 °C (see Fig. 6b for SW) is partly due to decomposition of the organic phenol formaldehyde-based binder present in SW [32]. Mg–Al layered double hydroxide (i.e., a hydrotalcite-like phase) might form in the developed binder in both fabricating techniques, in which the atomic ratio plots from SEM/EDS (shown in Fig. 5d and e) indicated a good linear correlation with a fixed Mg/Al ratio of roughly 1 (the slope of the cloud point). However, as reported in literature [30,33], Mg/Al atomic ratio was approximately 2 in slag-based AAMs for hydrotalcite-like hydrations. Accordingly, in Fig. 6, the slight mass loss between 200 and 400 °C could associate with the decomposition of hydrotalcite-like phase [30,34]. However, the presence of this phase was not clearly identified by XRD in this study (Fig. 4) due to its low crystallinity. As for PVA fiber, the fiber exhibited a slightly mass loss at 100–120 °C, due to coated oil in PVA fiber (approx. 1.2 wt% fiber as reported by Li et al. [35]) and absorbed moisture from hydrophilic nature of PVA. The fiber then started its decomposition at around 220 °C and up to 700 °C (Fig. 6c).

4.2. Mechanical properties

4.2.1. Flexural performance

The flexural strength of alkali-activated SW attained almost full development after 24 h in oven or 2–3 h of hot pressing (Fig. 8a). As for the unreinforced materials, the oven-cured 60/24 samples attained flexural strength approximately 3 MPa after 1 day, and strength remains in the same experimental scatter band after 40 and 60 days (Fig. 8a). It is worth noting that the plain material cured in oven exhibited some micro cracks due to high shrinkage (Fig. 7), which can have an additional negative impact on the flexural strength of the material. In contrast, there was no micro cracks observed on oven-cured and hot-pressed samples, the effects of fiber reinforcement and the combination of heat and pressure might reduce the risk of damages from shrinkage. In addition, the hot-pressed mixtures at 120 °C (120/2 and 120/3) reached around 4 MPa after demolding, and this is also its final-age strength. In contrast, 100/2 and 100/3 increased the flexural strength by roughly 75% after 40 and 60 days compared to that of after demolding. The difference is attributed to the lower heat provided in a relatively short pressing time, which leads to a lower degree of reaction at early age. As reported in Ref. [17], the increase in both pressing temperature and time offered a positive effect on dissolving of reactive portion of the aluminosilicate precursors of geopolymer.

PVA fibers greatly enhanced the flexural strength of reinforced mixtures as shown in Fig. 8b. The improvement ranged from 64.6% (120/3 vs. PVA-120/3 after 40 days) to 384.0% (60/24 vs. PVA-60/24 after 60 days). Additionally, there was no significant effect of pressing time in the flexural strength of reinforced samples at both 100° and 120 °C (Fig. 8b). Furthermore, the PVA fiber reinforced mixtures at 120 °C show a better flexural strength than that of 100 °C, and are comparable with the oven sample (in the same scatter band after 60 days). The reduction of flexural strength after 40 days of mixtures at 120 °C has not clear explanation. It could be connected to a random occurred residual distribution of pore water, not released with the higher temperature. As for the lower strength after heating at 100 °C (Fig. 8b), this could be attributed to a low degree of reaction. As discussed in Section 4.1, the main reaction product in all mixtures are C–(N–)A–S–H gel, and there are negligible differences among XRD patterns of oven-cured and hot-pressed materials. In addition, hot-pressed materials prepared at 120 °C seems to have less loosely bound water and pore water during sample preparation due to the high fabricating temperature. Therefore, further investigation is recommended to get insight into the

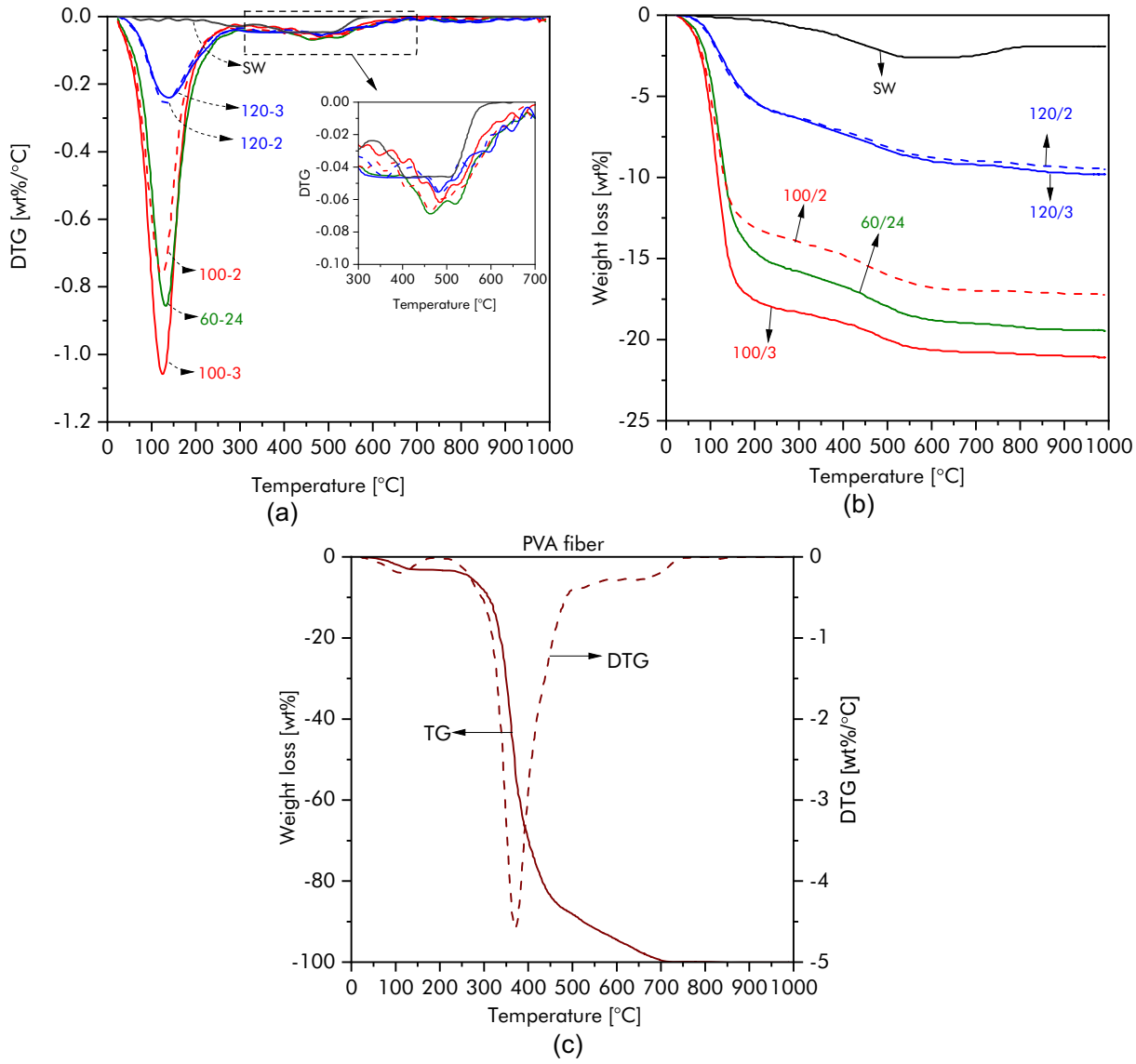

Fig. 6. (a) DTG and (b) TG curves of hot-pressed alkali-activated SW at different temperature (100 and 120 °C) and time (2 and 3 h) in comparison to the conventional alkali-activated one (60/24) and the raw material (SW), and (c) DTG and TG of PVA fiber.

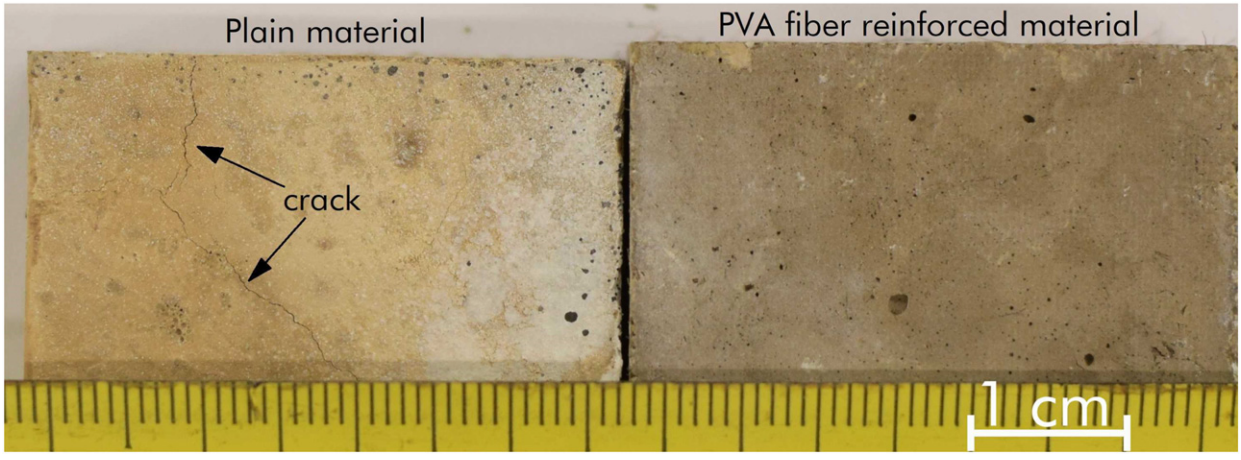

Fig. 7. Sample appearance of plain (left) and PVA fiber reinforced material (right) cured in oven; white color and black dots on the samples is the acrylic paint prepared for DIC testing.

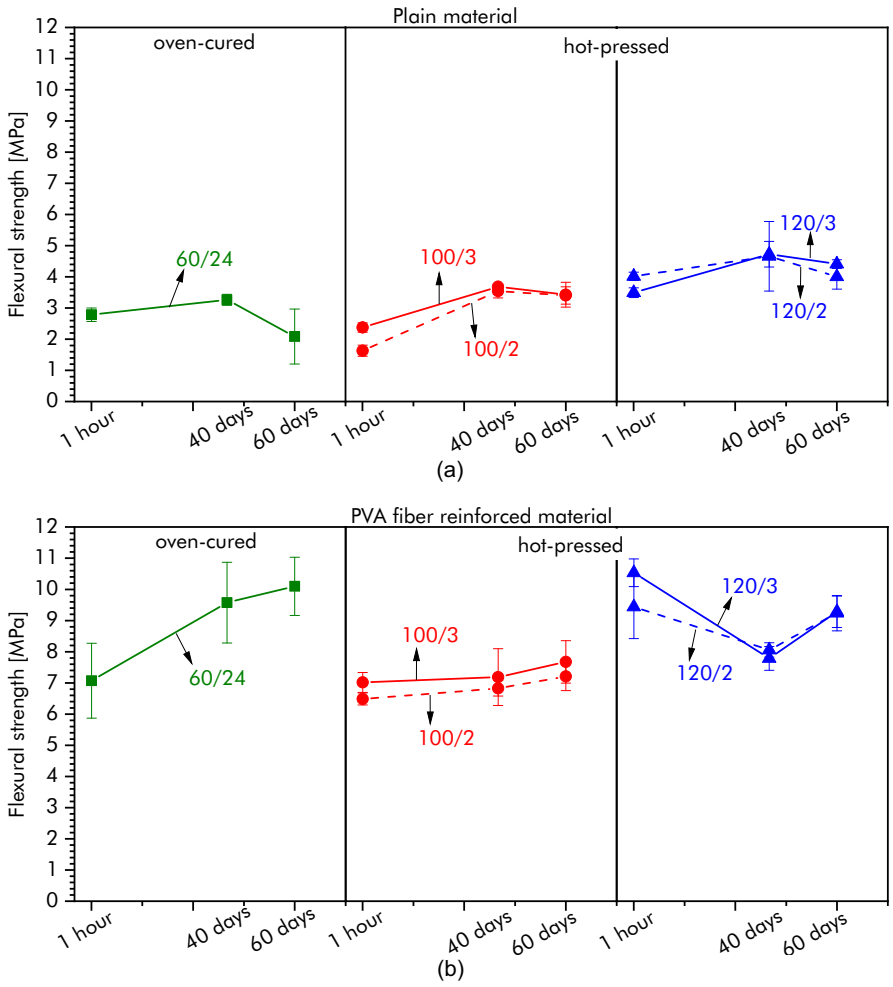

Fig. 8. Flexural strength of plain (a) and fiber reinforced (b) materials under 4-point bending after 1 h, 40 days and 60 days of hydration (error bars show standard deviation).

hydration and its products under hot-pressed conditions affecting the mechanical performance from micro to macro scale.

All PVA fiber reinforced compositions showed deflection hardening behavior under 4-point bending load, while plain materials exhibited brittle failure. Fig. 9 shows the bending response of all mixtures after demolding, 40, and 60 days of hydration. All plain compositions dropped loading level after reaching a peak load, which is a typical brittle failure. This failure was also indicated as a single crack observed at the peak load by DIC shown in Fig. 10. In contrast, all reinforced materials show deflection hardening behavior (Fig. 9, right). Eventually, this hardening behavior led to multiple cracks as shown in Fig. 10. As reported in Ref. [36], PVA fibers offered bridging action that helped transfer the load and delayed crack propagation. PVA fibers can be either pulled out or ruptured as observed in Ref. [37].

However, the properties of fiber under hot-pressing and eventually the interfacial bonding property between fibers and matrix might be affected. This could be reflected in the number of cracks observed by DIC (Fig. 10). The oven-cured and hot-pressed at 100 °C generated more cracks than that of hot-pressed at 120 °C. As discussed in Refs. [38,39], crack bridging is one of factors enhance the possibility of strain capacity and multiple cracking. Therefore, it can be seen that the number of cracks is an indicator to the efficiency of fiber bridging action. Although the PVA fibers are durable at relatively high pH, and start decomposition at approximately 220 °C (Fig. 6c for TG and DTG of PVA fiber), the combination of pressing temperature, pressure, and time seems to impart degradation of the fibers. Some evidence is shown and discussed in more details with SEM observation on the fracture surface of materials in Fig. 11.

The morphology of fracture surface showed good bonding between fibers and the matrix. Residual hydrated products are attached on the surface of the fiber (see SEM images in Fig. 11) due to the hydrophilic nature of PVA fibers. The good bonding between fibers and matrix allowed for an efficient load-carrying capacity and development of multiple cracks as shown in Figs. 9 and 10. Compared to the plain materials, larger amount of energy was absorbed in propagating cracks and eventually higher ductility was obtained in the reinforced composite. In addition, the unreacted needle-shaped particles can be clearly distinguished from the amorphous reaction product (Fig. 11b and c).

The 120 °C manufacturing process imparted damage in some fibers. Fig. 11d and e shows some burned out PVA fibers. This becomes particularly clear when comparing with the raw fibers (Fig. 1). In contrast, there was no obvious damages observed on PVA fiber at lower temperature (Fig. 11a–c). In literature, Wu and Li [40] reported that PVA fibers in reinforced cementitious composites have a rapidly decomposition under thermal exposure over 200 °C. Therefore, likely due to the combination of pressing temperature and time, the damaging of the fibers was in the very beginning at 120 °C with a pressure of 25 MPa. In addition, setup factors (e.g., pressure, time, and temperature) need further investigation to assess their role influencing on the kinetics of reaction of the aluminosilicates in the developed binder. Although the 120 °C process imparted damaged in some PVA fibers, the global mechanical response of the material was not affected with a good deflection hardening behavior (Fig. 9). However, the relationship between coupling of temperature and pressure and the level of damage in the fibers is worth to be investigated.

4.2.2. Flexural modulus of elasticity

Plain hot-pressed mixtures increased the modulus by hydration time in contrast to the oven-cured one. Fig. 12a distinguishes the flexural modulus of elasticity of all plain mixtures after 60 days of hydration. There was no significant difference between oven and hot-pressed curing conditions after demolding in terms of the modulus, all mixtures attained roughly from 1.5 to 2 GPa. However, after 40 and 60 days of hydration, the modulus of hot-pressed compositions increased significantly by 100–160% compared to the oven-cured material. The difference is attributed to further hydration of the hot-pressed mixtures at later stage. In contrast, the 60/24 mixture was cured in oven for 24 h and consequently its matrix is almost fully developed after that period. After 60 days of hydration, the flexural modulus retained comparable with samples after demolding at roughly 1.5 GPa.

Regarding reinforced compositions, all PVA fiber reinforced mixtures showed higher modulus than the plain mixtures (Fig. 12b). The flexural modulus was in a range of 4.5–5 GPa after demolding. In comparison to relevant plain mixtures, the modulus improved by roughly 25–150% with the presence of PVA. Furthermore, there was no significant change in terms of the modulus of reinforced materials after 40 and 60 days. The high modulus of PVA fiber (i.e., 41 GPa) and good bonding between fibers and matrix might contribute to this enhancement.

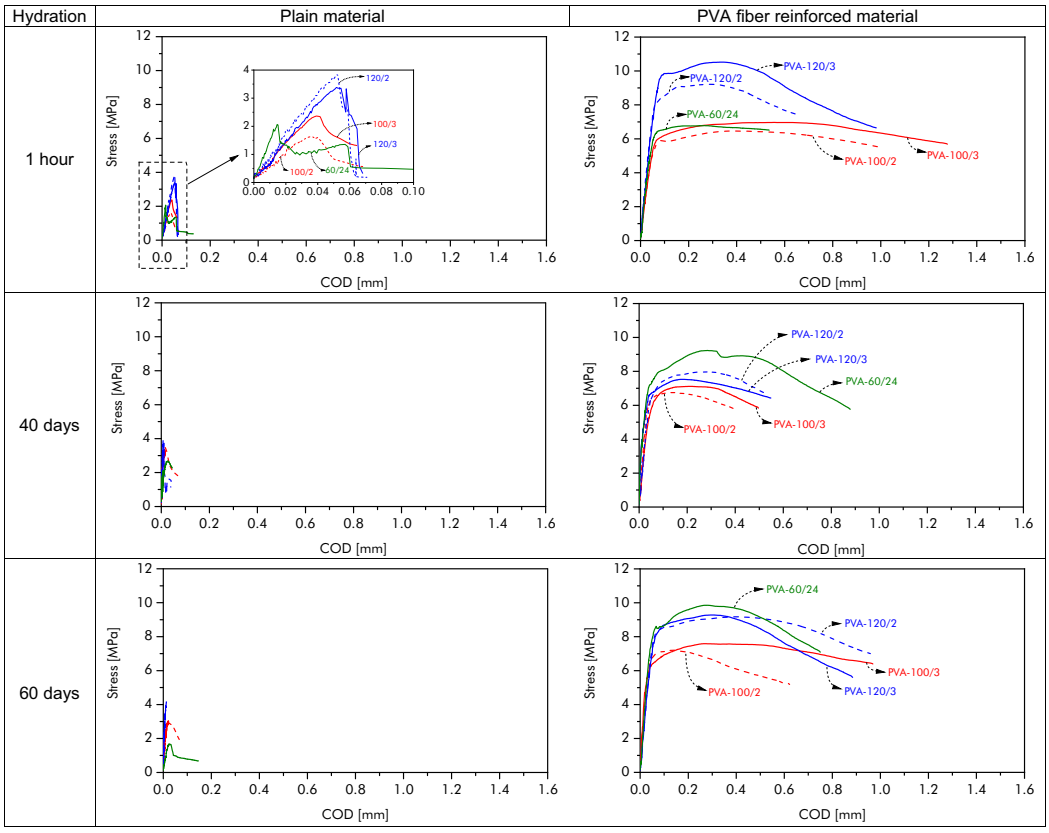

Fig. 9. Average flexural stress vs. COD curves of plain (left) and reinforced (right) materials under 4-point bending tests, after 1 h, 40 days, and 60 days of hydration.

4.2.3. Compressive strength

The PVA fibers improved the compressive strength of developed composites. Fig. 13 shows the compressive strength of plain and reinforced materials after 60 days of hydration. It can be seen that the fibers offered higher enhancement in hot-pressed mixtures than that of oven-cured compositions. PVA-60/24 increased by roughly 42% in comparison to the plain 60/24. In contrast, the increment of hot-press combinations ranged

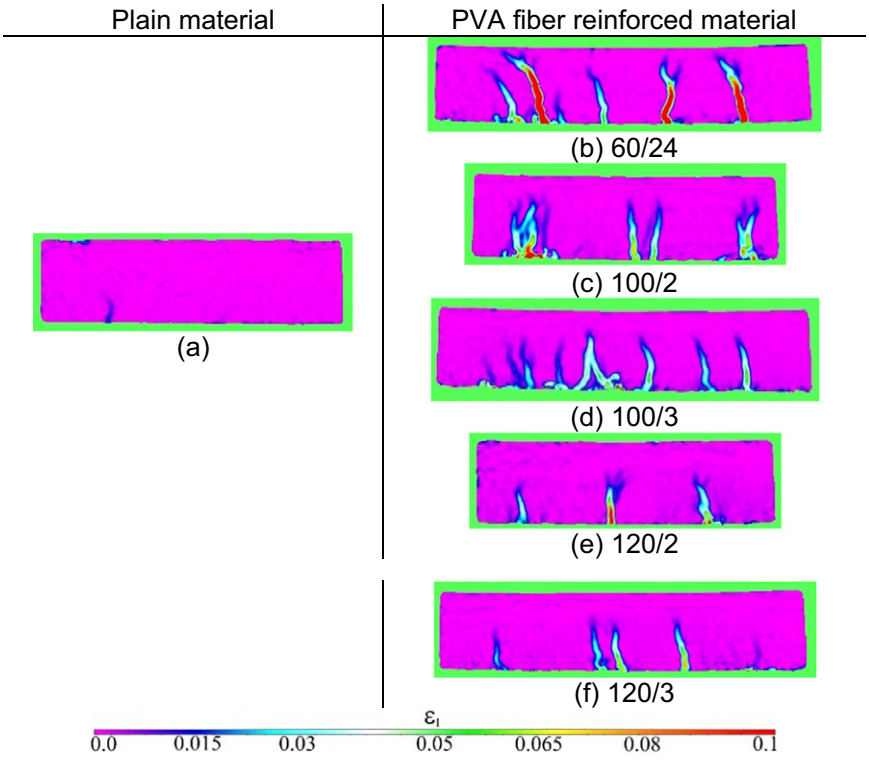

Fig. 10. Contour map of the maximum principal strain captured by the DIC technique at the peak load of all combinations: (a) the plain materials had typical brittle failure with a single crack and (b–f) multiple cracks of the PVA reinforced materials.

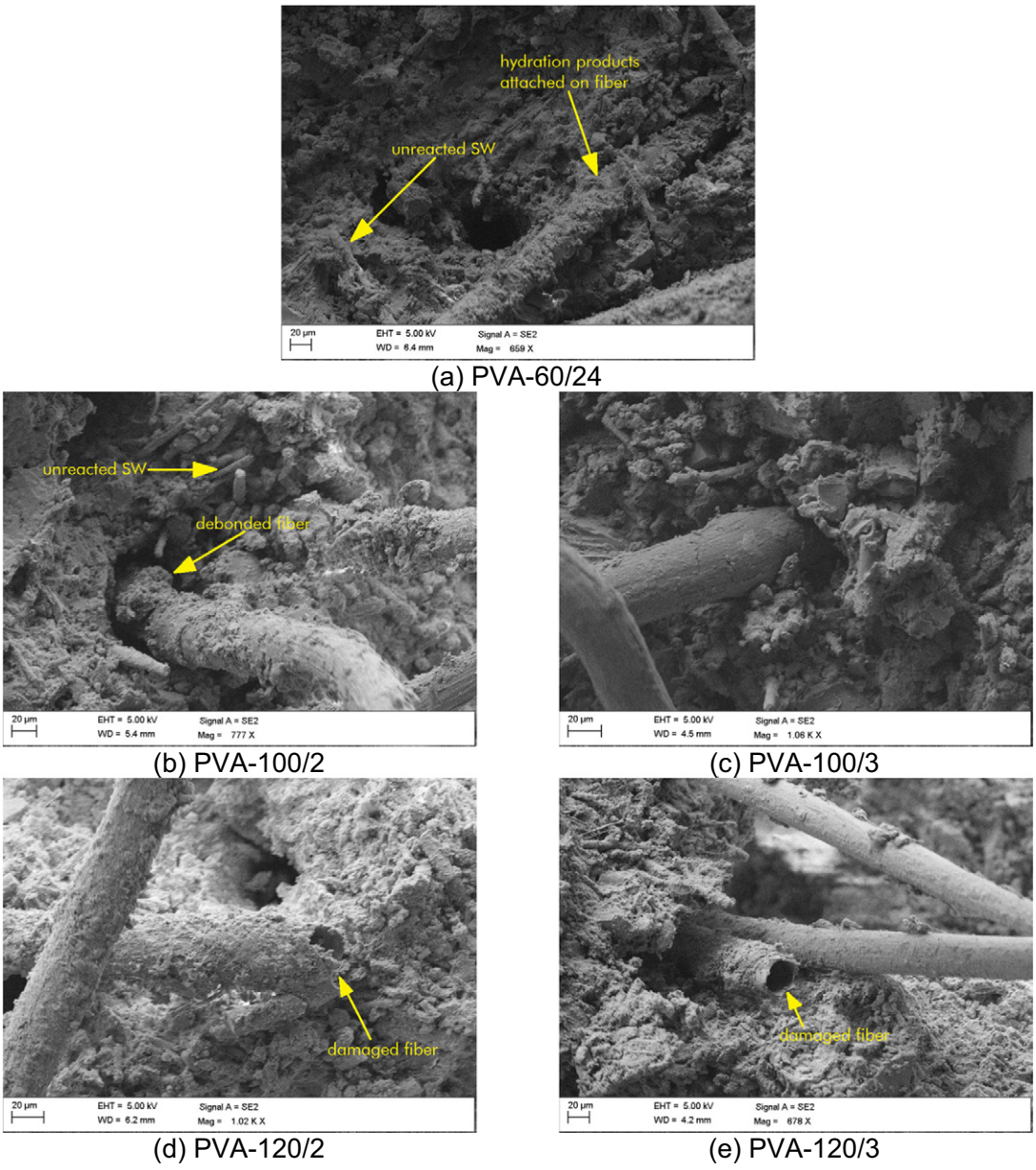

Fig. 11. SEM images of the fracture surface of PVA fiber reinforced alkali-activated SW after 60 days of hydration.

from 108% (for 3 h at 100 °C) to 137% (for 3 h at 120 °C). In addition, all reinforced mixtures attained approximately 35–40 MPa in compressive strength after 2 months irrespective of the fabricating method. However, the oven-cured plain material obtained slightly higher compressive strength compared to the hot-pressed unreinforced combination (Fig. 13a). As reported by Ranjbar [16], the compressive strength of hot-pressed fly ash based geopolymer could reach 134 MPa due to the synergic effects of pressure, temperature, and alkali activators. A longer pressing time at high temperature might have a drawback on the matrix (Figs. 13a, 120/3), namely lack of water for the hydration due to water evaporation. Since alkali activators play a very important role in the reaction of AAM [41,42], better understanding of the compensation effect of activators on hot-pressed AAM in fresh and hardened state properties is of interest for future study.

5. Life cycle assessment of the developed composites in laboratory scale

An estimation of the environmental impact of the considered materials was performed considering the CO_2 footprint and the energy consumption. Other indices are of interest for a complete estimation of the environmental impact (e.g. aquatic ecotoxicity, terrestrial ecotoxicity, etc.) here not considered as a scope of the research.

According to the standard ISO 14040 [43], the Life Cycle Assessment framework was selected in order to evaluate the environmental impact of the product. The procedure consists of four phases: (I) goal and scope definition, (II) life cycle inventory analysis, (III) life cycle impact assessment and (IV) results interpretation. The processes was assessed by the software SimaPro 8.3 [44], considering the method IMPACT 2002 + V2.13 [45]. The CO_2 emission ($kg_{CO2eq.}$) and the embodied energy ($MJ_{eq.}$) of the investigated materials and components were considered for comparison. The Eco Invent database [46] served as the primary source, for obtaining the life cycle inventory data of all manufacturing processes (LCA system boundaries) for 1 m^3 of produced material (functional unit).

However, some assumptions were made. First of all, the same oven from the database was chosen. To simulate the conventional oven or the hot-press, the energy consumption was modified for each scenario, starting from the selected process in the Ecolvent Database. It was assumed the devices are used at the highest electrical power during the time the materials were processed (5 kW for conventional oven, 6.4 kW for the hot-pressed). Furthermore, the different temperature

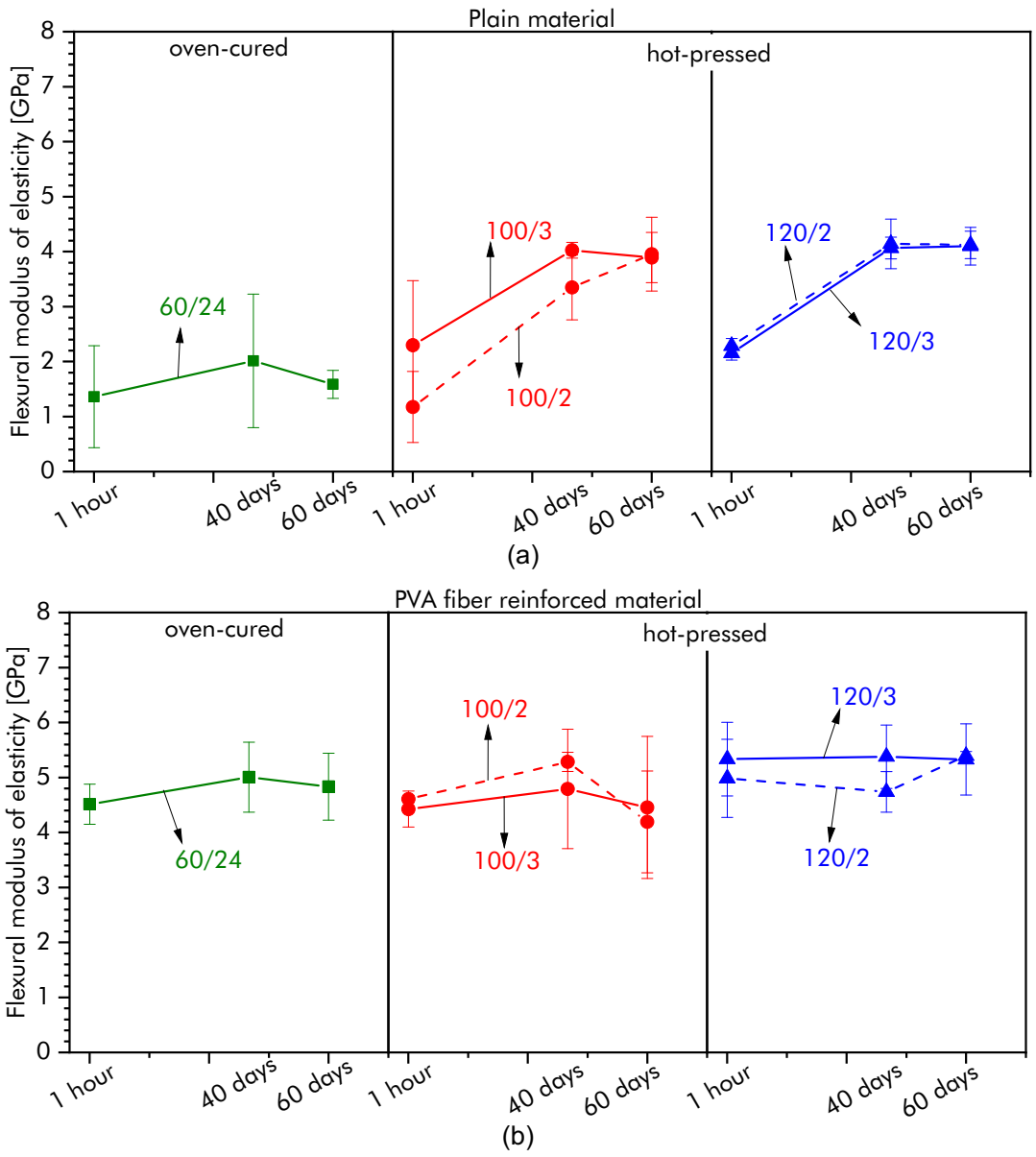

Fig. 12. Flexural modulus of elasticity of plain (a) and fiber reinforced (b) materials under 4-point bending after 1 h, 40 days, and 60 days of hydration (error bars show standard deviation).

of the devices could not be considered. To better estimate the effect of the temperature, a detailed knowledge of the time, heating variation and electric consumption should be available. However, it was not possible to record time and exact amount of electricity spend on the device. Thus, no difference between the temperatures could be made. Differences in molding technique was not considered since the pressing temperature used in this study is relatively low (i.e., 100 and 120 °C) compared to that of Ref. [16]. The mixing procedure was excluded from the calculation. Furthermore, the values of CO_2 emissions and embodied energy for PVA fibers were adopted from Ohno and Li [47]. It is worth noting that the energy consumption of milling raw material is the same for all mixtures and hence not considered in the assessment.

Table 5 shows the amount of raw ingredients for manufacturing of 1 m^3 of geopolymer in which the NaOH pellet and water were separated for the estimation in LCA. On basis of these data CO_2 footprint and embodied energy were calculated for each material, taking time and device of curing into consideration.

In general, geopolymer has a lower CO_2 emission per m^3 than OPC based engineered cementitious composite (OPC-based ECC). The main contributor in ECC is Portland cement making up 82% of the total emitted CO_2 (Fig. 14a). In Ref. [48], the published data has stated out two main reasons why the production of Portland cement has a high CO_2 release as much as 8% of global CO_2 emission. The first reason is the decomposition of carbonates (mainly $CaCO_3$) into oxides (largely lime, CaO) for the production of OPC clinker and CO_2. Secondly, the combustion of fossil fuels generates CO_2 and add a further 60% on top of the process emission [48]. Comparing SW based geopolymer and OPC-based ECC, oven-cured material had 45% less kg CO_2/m^3 than OPC-based ECC.

Focusing on the CO_2 emission of the geopolymer materials, the main contributor of them is the alkali activator NaOH with 46% (hot-pressed 2 h) – 37% (oven-cured 24 h). Moreover, hot-pressed materials had less CO_2 emission than oven produced materials with 18–20% lower CO_2 release than oven-cured material. The main reason for that is the duration of curing. The longer curing time in oven (24 h) emits more CO_2 than 2 or 3 h in hot press. However, the difference of global warming intensity (GWI) between 2 or 3 h in hot-press comparatively is almost 4 kg CO_2 per m^3.

Depending on the fiber and activator the embodied energy can have considerable variation among the materials (Fig. 14b). The contribution

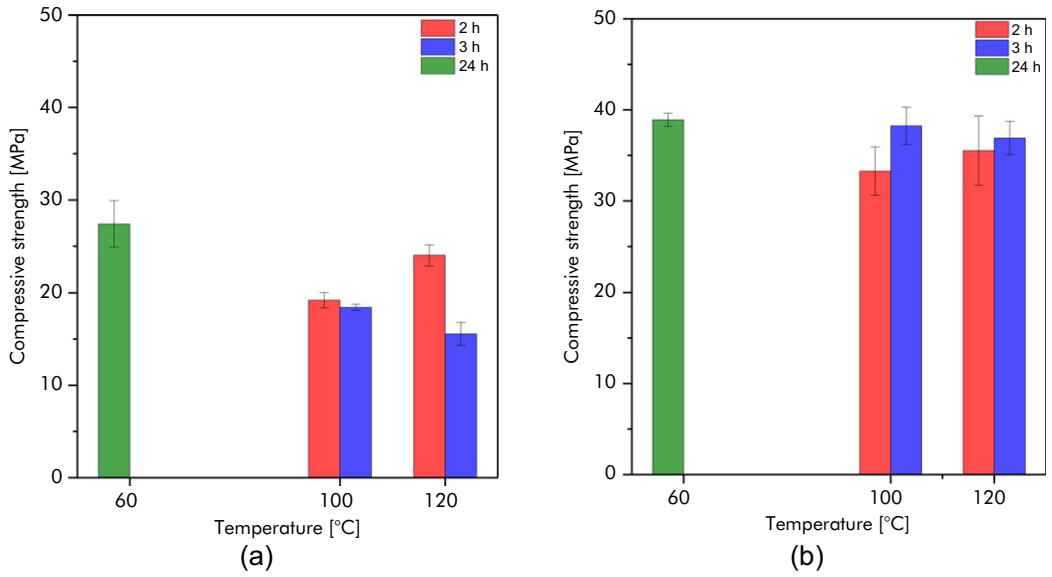

Fig. 13. Compressive strength of (a) plain material and (b) PVA fiber reinforced materials, after 60 days of hydration (error bars show standard deviation).

of the fiber is 35–40% of the total embodied energy, and 25–31% of CO_2. A more complicated production process of PVA fiber compared to other fibers (e.g., PP) can be one reason. This results in higher energy consumption and increases the embodied energy. Furthermore, NaOH accounts for 35–40% of the embodied energy. An attempt to lower the embodied energy can be the use of another activator with lower embodied energy and CO_2 emission as suggested in Ref. [49].

6. Multi-criteria ranking method

6.1. Description of the method

The method was adopted in previous work [50] and other works in the literature [51,52]. In this study, Equations (3)–(5) were used to rank all mixtures considering mechanical properties (i.e., flexural strength, flexural modulus, and compressive strength), embodied energy, and CO_2 emissions. The mechanical properties of all mixtures are reported in Section 4, while the LCA considering embodied energy and CO_2 footprint are detailed in Section 5. In the multi-criteria ranking method, a desirability function for each parameter is created resulting in a value between 0 and 1. It is clear that the mechanical properties of materials are favorable to the highest value (Equation (3)), while the embodied energy and CO_2 footprint are expected to be as low as possible (Equation (4)). The overall desirability function (Equation (5)) is then calculated to figure out the best and worst mixtures.

$$d_j = \frac{[Y_j - minf_j}{maxf_j - minf_j]_j^t} \tag{3}$$

$$d_j = \frac{[maxf_j - Y_j}{maxf_j - minf_j]_j^t} \tag{4}$$

Table 5
Recipe for 1 m^3 of alkali-activated SW (unit: kg).

Mixtures	SW	FS	PVA fiber	M100	Water	NaOH (pellet)	Total mass
Plain mixture	1050.05	315.02	0	5.82	568.74	113.76	2053.42
Reinforced mixture	1029.06	308.72	26	5.7	557.4	111.48	2038.37

$$D = (d_1 \times d_2 \times d_3 \times \ldots \times d_m)^{\frac{1}{m}} \tag{5}$$

where: Y_j is the result of the *j-th* parameter for a considered mixture; $minf_j$ and $maxf_j$ are the lowest and the highest results, respectively, of the *j-th* parameter over all the mixtures included in the ranking; t_j is a weighting factor of the *j-th* parameter; all weighting actors t_j are set to 1, so no parameter is more important than another; and m is the number of parameters.

6.2. Ranking and comparison

PVA fiber reinforced hot-pressed alkali-activated SW obtained top 3 highest ranked combinations. Fig. 15 shows the value of each considered parameter and the overall score of all mixture. It can be seen that fiber reinforced 120/3, 120/2, and 100/3 obtained the best balance between mechanical properties, cost, and environmental impact. In contrast, the oven-cured compositions obtained the lowest overall score due to its drawbacks in terms of embodied energy and CO_2 emission as discussed in Section 5 and shown in Fig. 14. Therefore, the hot-pressed technique has shown its advantages regarding lowering the energy spent to produce composites and CO_2 footprint. On the other hand, the hot-pressed combinations reached very high scores in compressive (0.86–0.97), flexural (0.7–0.9) strength, and flexural modulus (0.8–1). Consequently, manufacturing alkali-activated SW by hot-pressed technique resulted in advantages concerning CO_2 emission and embodied energy, while still gained high mechanical performance.

Combinations at 120 °C generally have a better ranking than that of 100 °C. The only exception is hot-pressed mixture at 120 °C for 3 h due to the lowest compressive strength of this mixture (score: 0). It is worth mentioning that the difference is mainly in mechanical properties, while other cost and greenhouse gas emission are comparable with other hot-pressed combinations (Fig. 15a). Therefore, it can be seen that this multi-criteria ranking method reveals some drawbacks as discussed in previous work [50]. Because the factors are multiplied for the overall function, a combination that contains one parameter with zero will result an overall score of 0 (e.g., 120/3). Therefore, it is suggested to adjust the weight of each factor in the ranking model to meet requirements with the design and application of materials. In this study, the focus was on a balanced weighting, meaning all criteria

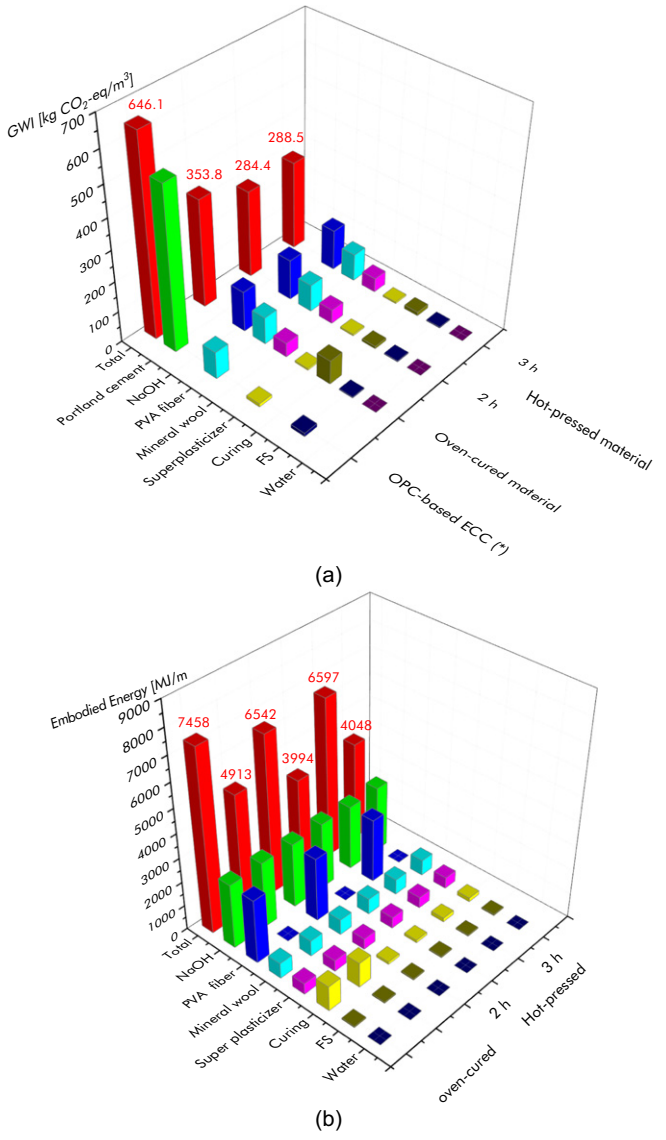

Fig. 14. (a) CO_2 footprint and (b) embodied energy of all combinations to produce 1 m^3 of materials; (*) data for OPC-based ECC was adopted from Ref. [47].

were considered with the same weight. However, if the mechanical properties play a major role in the application of material, the fiber reinforced oven-cured mixture can have the best ranking and is comparable with other hot-pressed mixtures. In addition, the ranking concerning mechanical properties shows good results as the weight is set to 0.9 out of 1.

7. Conclusions

This present study reports the manufacturing of fiber reinforced alkali-activated cementitious composites using hot-pressing technique. The developed composite mixtures can attain almost final strength after 2–3 h of pressing at 100–120 °C. In addition, the PVA fiber reinforced composite exhibited deflection hardening behavior with comparable mechanical performance to that of conventional oven-cured alkali-activated SW. Therefore, this technique can shorten the molding time in production, while still attaining high mechanical performance. This opens possibility to increase the productivity of pre-cast fiber reinforced alkali-activated materials, although the limitation to specific shapes of hot press manufacturing.

The results from XRD and DTG analysis shows that the main reaction product of all mixtures is probably amorphous C–(N–)A–S–H gel. There was no significant difference in terms of mineralogy between hot-pressed and oven cured mixtures. However, some further investigations are suggested to get insight into the effects of hot-pressed technique on the reaction products and phase assemblage of alkali-activated materials.

According to LCA output considering at laboratory scale, the main contributor of CO_2 emission in the developed mixtures is the alkali activator NaOH. Between the two fabricating techniques, the hot-pressed released less CO_2 emission than the oven-produced materials by 18–20%. The main reason is due to the shorter curing duration. In addition, the embodied energy of mixtures can vary depending on fiber type and activator. It is worth noting that the contribution of PVA fiber and NaOH in a mixture can range roughly 35–40% of the total embodied energy. Therefore, other activators or fiber reinforcement are of interest to reduce the energy and greenhouse gas emission.

The multi-criteria ranking method suggested hot-pressed fiber reinforced 120/2, 120/3, and 100/3 as the top 3 best mixtures obtaining the balance between mechanical properties, cost, and environmental impact. This confirms the advantages of hot-pressed technique in comparison to the conventional oven-cured for low-CaO alkali-activated material. In addition, among hot-pressed mixtures, combinations manufactured at higher temperature seems to be more favorable and higher ranked. However, at 120 °C, some damages on PVA fibers were observed by SEM. This leads to a need for future investigations in terms of the effects of hot-pressed conditions on micro structure of materials and the interaction between fiber and matrix.

CRediT authorship contribution statement

Hoang Nguyen: Conceptualization, Data curation, Formal analysis, Investigation, Methodology, Visualization, Writing - original draft, Writing - review & editing. **Alexandra Kaas:** Data curation, Formal analysis, Investigation, Visualization, Writing - review & editing. **Paivo Kinnunen:** Investigation, Visualization, Writing - review & editing, Supervision. **Valter Carvelli:** Formal analysis, Validation, Investigation, Writing - review & editing. **Carol Monticelli:** Data curation, Formal analysis, Writing - review & editing. **Juho Yliniemi:** Project administration, Resources, Funding acquisition, Formal analysis, Writing - review & editing. **Mirja Illikainen:** Writing - review & editing, Supervision, Funding acquisition.

Acknowledgements

This work was done under:

- GEODESIGN (project number: 1215/31/2015) funded by Business Finland and companies Boliden Harjavalta Oy, Destaclean Oy, Fortum Power and Heat Oy, Paroc Group Oy, Saint-Gobain Finland Oy, and Suomen Erityisjäte Oy.
- FLOW (project number: 8904/31/2017) project funded by Business Finland in the ERA-MIN 2 Innovation program, which is part of the EU Horizon 2020 program.

The authors gratefully acknowledge Jatin Sethi (KTH Royal Institute of Technology, Sweden), Maiju Hietala (University of Oulu, Finland) for the help of operating hot-pressed machine. In the University of Oulu, the help of Tero Luukkonen, Jarno Karvonen, Elisa Wirkkala, Patrick L. Ninla, Tommi Kokkonen, and Pasi Juntunen during lab work is appreciated.

Data availability

The raw/processed data required to reproduce these findings cannot be shared at this time as the data also forms part of an ongoing study.

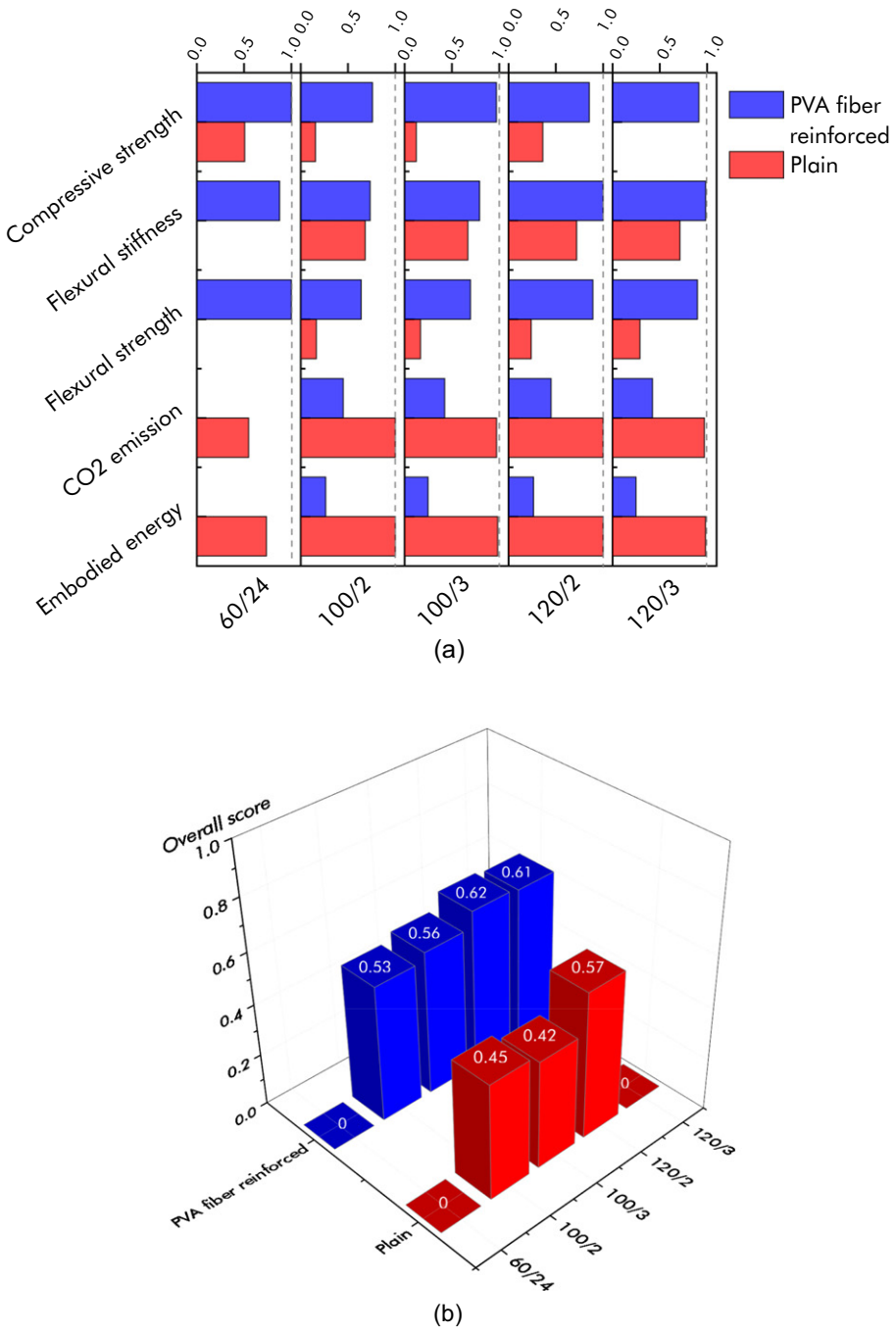

Fig. 15. (a) Individual and (b) overall desirable functions of the mixtures based on the multi-criteria ranking method.

Appendix A. Supplementary data

Supplementary data to this article can be found online at https://doi.org/10.1016/j.matdes.2019.108315.

References

[1] P. Duxson, J.L. Provis, G.C. Lukey, J.S.J. van Deventer, The role of inorganic polymer technology in the development of 'green concrete, Cement Concr. Res. 37 (2007) 1590–1597, https://doi.org/10.1016/j.cemconres.2007.08.018.
[2] J.S.J. van Deventer, J.L. Provis, P. Duxson, D.G. Brice, Chemical research and climate change as drivers in the commercial adoption of alkali activated materials, Waste Biomass Valorization 1 (2010) 145–155, https://doi.org/10.1007/s12649-010-9015-9.
[3] Y. Ding, J.-G. Dai, C.-J. Shi, Mechanical properties of alkali-activated concrete: a state-of-the-art review, Constr. Build. Mater. 127 (2016) 68–79, https://doi.org/10.1016/j.conbuildmat.2016.09.121.
[4] G. Xu, X. Shi, Characteristics and applications of fly ash as a sustainable construction material: a state-of-the-art review, Resour. Conserv. Recycl. 136 (2018) 95–109, https://doi.org/10.1016/j.resconrec.2018.04.010.
[5] O. Väntsi, T. Kärki, Mineral wool waste in Europe: a review of mineral wool waste quantity, quality, and current recycling methods, J. Mater. Cycles Waste Manag. (2013) (2013) 1–11, https://doi.org/10.1007/s10163-013-0170-5.
[6] A.M. Papadopoulos, State of the art in thermal insulation materials and aims for future developments, Energy Build. 37 (2005) 77–86, https://doi.org/10.1016/j.enbuild.2004.05.006.
[7] V.C. Li, On engineered cementitious composites (ECC), J. Adv. Concr. Technol. 1 (2003) 215–230, https://doi.org/10.3151/jact.1.215.
[8] V.C. Li, D.K. Mishra, H.-C. Wu, Matrix design for pseudo-strain-hardening fibre reinforced cementitious composites, Mater. Struct. 28 (1995) 586–595, https://doi.org/10.1007/BF02473191.

[9] V. Afroughsabet, L. Biolzi, T. Ozbakkaloglu, High-performance fiber-reinforced concrete: a review, J. Mater. Sci. 51 (2016) 6517–6551, https://doi.org/10.1007/s10853-016-9917-4.
[10] S.H. Said, H.A. Razak, The effect of synthetic polyethylene fiber on the strain hardening behavior of engineered cementitious composite (ECC), Mater. Des. 86 (2015) 447–457, https://doi.org/10.1016/j.matdes.2015.07.125.
[11] M.A.E.M. Ali, A.M. Soliman, M.L. Nehdi, Hybrid-fiber reinforced engineered cementitious composite under tensile and impact loading, Mater. Des. 117 (2017) 139–149, https://doi.org/10.1016/j.matdes.2016.12.047.
[12] B. Nematollahi, J. Sanjayan, F.U.A. Shaikh, Matrix design of strain hardening fiber reinforced engineered geopolymer composite, Compos. B Eng. 89 (2016) 253–265, https://doi.org/10.1016/j.compositesb.2015.11.039.
[13] H. Nguyen, V. Carvelli, E. Adesanya, P. Kinnunen, M. Illikainen, High performance cementitious composite from alkali-activated ladle slag reinforced with polypropylene fibers, Cement Concr. Compos. 90 (2018) 150–160, https://doi.org/10.1016/j.cemconcomp.2018.03.024.
[14] W. Dong, W. Li, L. Shen, D. Sheng, Piezoresistive behaviours of carbon black cement-based sensors with layer-distributed conductive rubber fibres, Mater. Des. 182 (2019) 108012, https://doi.org/10.1016/j.matdes.2019.108012.
[15] S. Chaves Figueiredo, C. Romero Rodríguez, Z.Y. Ahmed, D.H. Bos, Y. Xu, T.M. Salet, O. Çopuroğlu, E. Schlangen, F.P. Bos, An approach to develop printable strain hardening cementitious composites, Mater. Des. 169 (2019) 107651, https://doi.org/10.1016/j.matdes.2019.107651.
[16] N. Ranjbar, M. Mehrali, M.R. Maheri, M. Mehrali, Hot-pressed geopolymer, Cement Concr. Res. 100 (2017) 14–22, https://doi.org/10.1016/j.cemconres.2017.05.010.
[17] N. Ranjbar, A. Kashefi, M.R. Maheri, Hot-pressed geopolymer: dual effects of heat and curing time, Cement Concr. Compos. 86 (2018) 1–8, https://doi.org/10.1016/j.cemconcomp.2017.11.004.
[18] N. Ranjbar, Ultra-high Strength Hot-Pressed Geopolymeric Composition and Production Method Thereof, US20180244572, 2018.
[19] J.L. Provis, Alkali-activated materials, Cement Concr. Res. (2017) https://doi.org/10.1016/j.cemconres.2017.02.009.
[20] J.L. Provis, J.S.J. van Deventer, 16 - geopolymers and other alkali-activated materials, in: P.C. Hewlett, M. Liska (Eds.), Leas Chem. Cem. Concr, fifth ed.Butterworth-Heinemann 2019, pp. 779–805, https://doi.org/10.1016/B978-0-08-100773-0.00016-2.
[21] R. Taylor, I.G. Richardson, R.M.D. Brydson, Composition and microstructure of 20-year-old ordinary Portland cement–ground granulated blast-furnace slag blends containing 0 to 100% slag, Cement Concr. Res. 40 (2010) 971–983, https://doi.org/10.1016/j.cemconres.2010.02.012.
[22] Thermodynamic modelling of alkali-activated slag cements, Appl. Geochem. 61 (2015) 233–247, https://doi.org/10.1016/j.apgeochem.2015.06.006.
[23] C. Kuenzel, N. Ranjbar, Dissolution mechanism of fly ash to quantify the reactive aluminosilicates in geopolymerisation, Resour. Conserv. Recycl. 150 (2019) 104421, https://doi.org/10.1016/j.resconrec.2019.104421.
[24] ISO 13320:2009 - Particle Size Analysis – Laser Diffraction Methods. , International Organization for Standardization, 2009.
[25] M. Sahmaran, M. Lachemi, K.M.A. Hossain, R. Ranade, V.C. Li, Influence of aggregate type and size on ductility and mechanical properties of engineered cementitious composites, Mater. J. 106 (2009) https://doi.org/10.14359/56556.
[26] J.H. Flynn, Chapter 14 - polymer degradation, in: S.Z.D. Cheng (Ed.), Handb. Therm. Anal. Calorim. Elsevier Science B.V. 2002, pp. 587–651, https://doi.org/10.1016/S1573-4374(02)80017-6.
[27] ASTM International, ASTM C1609/C1609M, Standard Test Method for Flexural Performance of Fiber-Reinforced Concrete (Using Beam with Third-Point Loading), ASTM International, West Conshohocken, PA, 2015. www.astm.org.
[28] ISO Committee, ISO 14125:1998, Fibre-Reinforced Plastic Composites – Determination of Flexural Properties, ISO Committee, Geneva, 2013. https://www.iso.org/standard/23637.html.
[29] LaVision StrainMaster, http://www.lavision.de/en/products/strainmaster/index.php 2016, Accessed date: 27 January 2017.
[30] M.B. Haha, B. Lothenbach, G. Le Saout, F. Winnefeld, Influence of slag chemistry on the hydration of alkali-activated blast-furnace slag — Part I: effect of MgO, Cement Concr. Res. 41 (2011) 955–963, https://doi.org/10.1016/j.cemconres.2011.05.002.
[31] S.A. Bernal, E.D. Rodríguez, R.M. Gutiérrez, M. Gordillo, J.L. Provis, Mechanical and thermal characterisation of geopolymers based on silicate-activated metakaolin/slag blends, J. Mater. Sci. 46 (2011) 5477–5486, https://doi.org/10.1007/s10853-011-5490-z.
[32] J. Yliniemi, P. Kinnunen, P. Karinkanta, M. Illikainen, Utilization of mineral wools as alkali-activated material precursor, mater, Basel Switz 9 (2016) 312, https://doi.org/10.3390/ma9050312.
[33] A. Machner, M. Zajac, M. Ben Haha, K.O. Kjellsen, M.R. Geiker, K. De Weerdt, Limitations of the hydrotalcite formation in Portland composite cement pastes containing dolomite and metakaolin, Cement Concr. Res. 105 (2018) 1–17, https://doi.org/10.1016/j.cemconres.2017.11.007.
[34] S.-D. Wang, K.L. Scrivener, P.L. Pratt, Factors affecting the strength of alkali-activated slag, Cement Concr. Res. 24 (1994) 1033–1043, https://doi.org/10.1016/0008-8846(94)90026-4.
[35] V.C. Li, C. Wu, S. Wang, A. Ogawa, T. Saito, Interface tailoring for strain-hardening polyvinyl alcohol-engineered cementitious composite (PVA-ECC), Mater. J. 99 (2002) 463–472, https://doi.org/10.14359/12325.
[36] E.-H. Yang, S. Wang, Y. Yang, V.C. Li, Fiber-bridging constitutive law of engineered cementitious composites, J. Adv. Concr. Technol. 6 (2008) 181–193, https://doi.org/10.3151/jact.6.181.
[37] M. Nedeljković, M. Luković, K. van Breugel, D. Hordijk, G. Ye, Development and application of an environmentally friendly ductile alkali-activated composite, J. Clean. Prod. 180 (2018) 524–538, https://doi.org/10.1016/j.jclepro.2018.01.162.
[38] J. Zhang, C.K.Y. Leung, Y. Gao, Simulation of crack propagation of fiber reinforced cementitious composite under direct tension, Eng. Fract. Mech. 78 (2011) 2439–2454, https://doi.org/10.1016/j.engfracmech.2011.06.003.
[39] C. Lu, C.K.Y. Leung, V.C. Li, Numerical model on the stress field and multiple cracking behavior of Engineered Cementitious Composites (ECC), Constr. Build. Mater. 133 (2017) 118–127, https://doi.org/10.1016/j.conbuildmat.2016.12.033.
[40] C. Wu, V.C. Li, Thermal-mechanical behaviors of CFRP-ECC hybrid under elevated temperatures, Compos. B Eng. 110 (2017) 255–266, https://doi.org/10.1016/j.compositesb.2016.11.037.
[41] N. Li, C. Shi, Z. Zhang, Understanding the roles of activators towards setting and hardening control of alkali-activated slag cement, Compos. B Eng. (2019) https://doi.org/10.1016/j.compositesb.2019.04.024.
[42] D. Ravikumar, N. Neithalath, Effects of activator characteristics on the reaction product formation in slag binders activated using alkali silicate powder and NaOH, Cement Concr. Compos. 34 (2012) 809–818, https://doi.org/10.1016/j.cemconcomp.2012.03.006.
[43] ISO Committee, ISO 14040 - Environmental Management - Life Cycle Assessment - Principles and Framework, ISO Committee, Geneva, 2006.
[44] SimaPro | the world's leading LCA software, SimaPro. (n.d.) https://simapro.com/, Accessed date: 13 February 2019.
[45] O. Jolliet, M. Margni, R. Charles, S. Humbert, J. Payet, G. Rebitzer, R. Rosenbaum, Impact 2002+: a new life cycle impact assessment methodology, Int. J. Life Cycle Assess. 8 (2003) 324, https://doi.org/10.1007/BF02978505.
[46] , Ecoinvent Version 3, (n.d.) https://www.ecoinvent.org/database/database.html, Accessed date: 13 February 2019.
[47] M. Ohno, V.C. Li, An integrated design method of Engineered Geopolymer Composite, Cement Concr. Compos. 88 (2018) 73–85, https://doi.org/10.1016/j.cemconcomp.2018.02.001.
[48] R.M. Andrew, Global CO2 emissions from cement production, Earth Syst. Sci. Data 10 (2018) 195–217, https://doi.org/10.5194/essd-10-195-2018.
[49] A. Passuello, E.D. Rodríguez, E. Hirt, M. Longhi, S.A. Bernal, J.L. Provis, A.P. Kirchheim, Evaluation of the potential improvement in the environmental footprint of geopolymers using waste-derived activators, J. Clean. Prod. 166 (2017) 680–689, https://doi.org/10.1016/j.jclepro.2017.08.007.
[50] H. Nguyen, M. Staudacher, P. Kinnunen, V. Carvelli, M. Illikainen, Multi-fiber reinforced ettringite-based composites from industrial side streams, J. Clean. Prod. 211 (2019) 1065–1077, https://doi.org/10.1016/j.jclepro.2018.11.241.
[51] M. Mastali, A. Dalvand, A.R. Sattarifard, M. Illikainen, Development of eco-efficient and cost-effective reinforced self-consolidation concretes with hybrid industrial/recycled steel fibers, Constr. Build. Mater. 166 (2018) 214–226, https://doi.org/10.1016/j.conbuildmat.2018.01.147.
[52] O. Sengul, Mechanical behavior of concretes containing waste steel fibers recovered from scrap tires, Constr. Build. Mater. 122 (2016) 649–658, https://doi.org/10.1016/j.conbuildmat.2016.06.113.